Chapter 16

Challenges for 100 Milligram Flapping Flight

Ronald S. Fearing and Robert J. Wood

Abstract Creating insect-scale flapping flight at the 0.1 gram size has presented significant engineering challenges. A particular focus has been on creating miniature machines which generate similar wing stroke kinematics as flies or bees. Key challenges have been thorax mechanics, thorax dynamics, and obtaining high power-to-weight ratio actuators. Careful attention to mechanical design of the thorax and wing structures, using ultra-high-modulus carbon fiber components, has resulted in high-lift thorax structures with wing drive frequencies at 110 and 270 Hz. Dynamometer characterization of piezoelectric actuators under resonant load conditions has been used to measure real power delivery capability. With currently available materials, adequate power delivery remains a key challenge, but at high wingbeat frequencies, we estimate that greater than 400 W/kg is available from PZT bimorph actuators. Neglecting electrical drive losses, a typical 35% actuator mass fraction with 90% mechanical transmission efficiency would yield greater than 100 W/kg wing shaft power. Initially the micromechanical flying insect (MFI) project aimed for independent control of wing flapping and rotation using two actuators per wing. At resonance of 270 Hz, active control of a 2 degrees of freedom wing stroke requires precise matching of all components. Using oversized actuators, a bench top structure has demonstrated lift greater than 1000 μN from a single wing. Alternatively, the thorax structure can be drastically simplified by using passive wing rotation and a single-drive actuator. Recently, a 60 mg flapping-wing robot using passive wing rotation has taken off for the first time using external power and guide rails.

R.S. Fearing (✉)
Biomimetic Millisystems Lab, Univ. of California, Berkeley, CA, USA
e-mail: ronf@eecs.berkeley.edu

16.1 Motivation and Background

Flies (order Diptera) are arguably the most agile objects on earth, including all things man-made and biological. They can fly in any direction, make 90° turns in tens of milliseconds, land on walls and ceilings, and navigate very complex environments. It is natural then to use flies as inspiration for a small autonomous flying robot. However, this bio-inspiration must be done with care. There are certain aspects of insect morphology and physiology which would not make sense to replicate (reproduction, for example). So our bio-inspiration paradigm hopes to observe natural systems and extract the underlying principles. Then we apply our most advanced engineering techniques in concert with these principles to achieve a desired goal.

Insects control flight with a three degrees of freedom (DOF) wing motion and either one or two pairs of wings. This discussion focuses on two-wing insects for two reasons: first, the agility of Dipteran insects is arguably rivaled only by a few species of Odonata. Second, the mechanical complexity of four wings is simply greater than that of two. The three DOF wing trajectory consists of flapping, rotation, and stroke plane deviation. Flapping (upstroke and downstroke) defines the stroke plane. Rotation consists of pronation and supination about an axis parallel to the spanwise direction. The final DOF is stroke plane deviation; however, this will not be considered due to the fact that hovering Dipteran wing motions can be approximately characterized with only two rotational axes.

D. Floreano et al. (eds.), *Flying Insects and Robots*,
DOI 10.1007/978-3-540-89393-6_16,

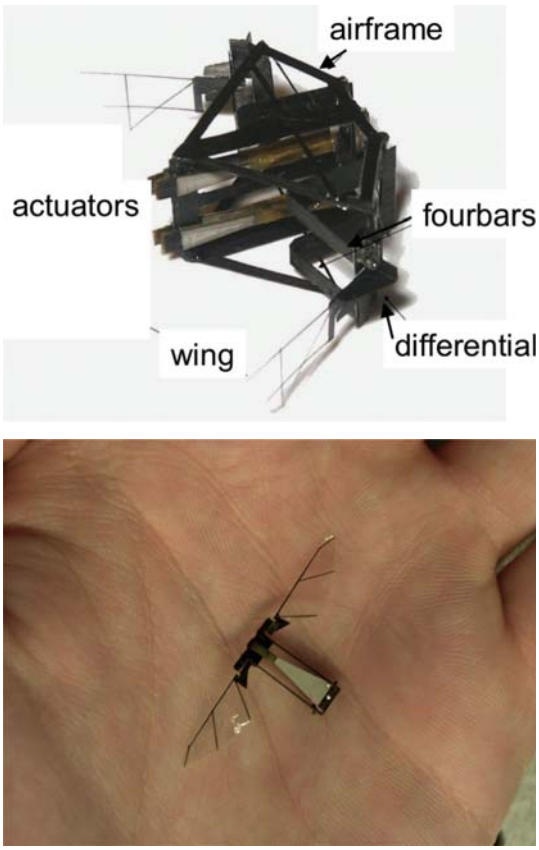

Fig. 16.1 Prototype flapping-wing MAVs, with integrated air frame, thorax, and piezoelectric actuators, but offboard power. (**a**) UC Berkeley micromechanical flying insect (130 mg). (**b**) Harvard microrobotic fly (60 mg)

This periodic wing trajectory exists at a Reynolds number of approximately 100–1000 and thus the flow around the wings is mostly separated. Biologists have identified key features of the flow patterns of hovering Diptera and collectively called these 'unsteady aerodynamics' [8, 17]. No closed-form analytical description of the unsteady aerodynamics exists due to the challenges in capturing all fluid interactions with non-trivial airfoil deformations. Moreover, the vast diversity in wing morphology (e.g., shapes, textures, anisotropic compliance) offers a further impediment to a simple description of flapping-wing flight [5, 6]. Similarly, numerical simulations (solving the Navier–Stokes equations) have proven difficult for broad studies of multiple simultaneous unsteady aerodynamics phenomena. However, simplified wing models and kinematics have been used to explain some aspects of insect flight [18]. Finally, dynamically scaled robotic insect wings have resulted in approximate quasi-steady empirical models using lift and drag coefficients to hide the unsteady terms [8]. These empirically derived models are used throughout the design of a robotic fly due to their relative simplicity. These models provide the engineer with a first-order approximation to the forces and moments expected from a pair of flapping wings.

This chapter will describe the design and fabrication of two classes of robotic flies, shown in Fig. 16.1, using characteristics and models derived from insect flight.

16.2 Design of High-Frequency Flapping Mechanisms

Diptera have two sets of flight muscles: direct and indirect [10] as shown in Fig. 16.2. The indirect flight muscles control flapping and provide the vast majority of power for flight [9]. The direct flight muscles insert directly on the pleural wing process via basalar sclerites [13]. It is thought, therefore, that the direct flight muscles are involved with control of pronation and supination of the wing. Details of insect wing drive systems are provided in Chap. 15.

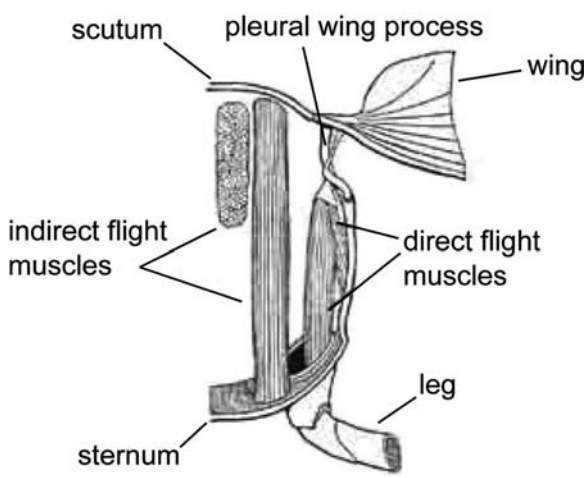

Fig. 16.2 Simplified drawing of a Dipteran thorax. The indirect flight muscles (dorsoventral and dorsolongitudinal) create the upstroke and downstroke, respectively. The direct flight muscles insert on the base of the wing hinge at the pleural wing process (adapted from [10])

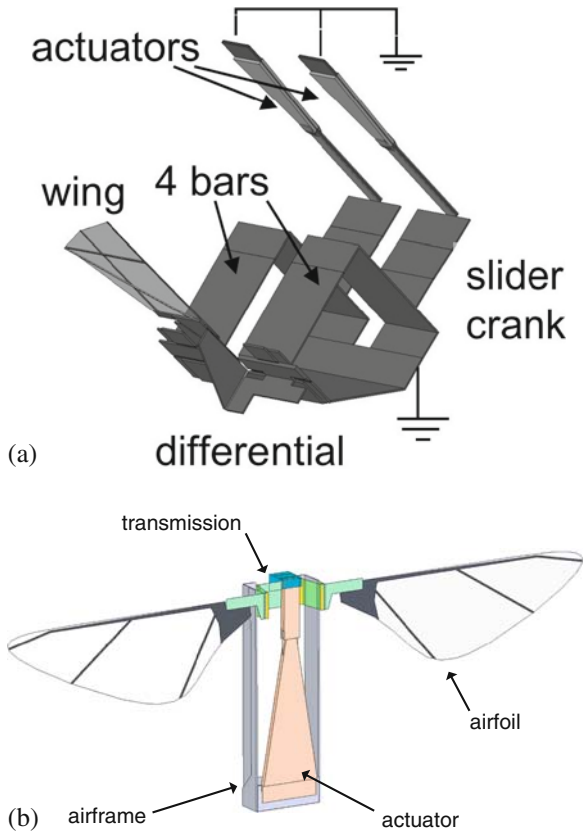

Fig. 16.3 (**a**) Half of original four actuator thorax with two independent DOF per wing [14]. (**b**) Simplified thorax with single-drive actuator and passive wing rotation [19]

The first design for a flapping-wing MAV (Fig. 16.3a) combines power and flight control actuators to provide direct control of pronation and supination. However, it is speculated that dynamic forces acting on the wing during flight also contribute to wing rotation [12]. The second design for a flapping-wing MAV (Fig. 16.3b) uses this latter assumption and relies on passive wing rotation.

16.2.1 Four Actuator Thorax

A wing drive mechanism was designed to provide simultaneous control of wing flapping and rotation angles using a two-input two-output transmission system shown in Fig. 16.3a. To minimize reactive power required to drive the wing inertia, the thorax is designed to operate near mechanical resonance as described by Avadhanula et al. [2]. Each wing is driven by two piezoelectric bimorph bending actuators [22], which provide an unloaded displacement of $\pm$ 250 μm and blocked force of $\pm$ 60 mN [22]. The transmission is designed [14, 15, 20, 3] to convert this high-force small displacement to an ideal wing stroke of $\pm$ 60°, with an equivalent transmission ratio of approximately 3000 rad m^{-1}.

The MFI structure in Fig. 16.3a uses two stages of mechanical amplification followed by a differential element to couple the individual actuator motion into wing flapping and rotation. The first stage slider-crank converts actuator linear displacement into $\pm$ 10° input to the planar four bar. The four bar has a nominal amplification of 6:1, providing an ideal $\pm$ 60° output motion. Finally, the two planar four bars are coupled into a spherical five-bar differential element [2, 3], an approximation to the insect wing hinge. The differential element converts angle difference between the four bars into wing rotation, such that a 22° angle difference gives rise to a 45° wing rotation. The original goal of this design was to achieve independent control of flapping and rotation, providing much greater control moments than even real insects can obtain. As discussed in Sect. 16.6.1, wing inertial and aerodynamic coupling effects dominate the available actuator control effort, making independent control difficult to achieve. The lessons learned from the four actuator MFI motivated the design of a structure with greatly reduced complexity, described next.

16.2.2 Single Actuator Thorax with Passive Rotation

The design of a flapping-wing MAV based on passive rotation is shown in Fig. 16.3b. Here a central power actuator is responsible for controlling flapping while pronation and supination are passive. The power actuator thus acts to deliver a maximal amount of power to the wing stroke in an analogous fashion to the indirect flight muscles of the Dipteran thorax. Passive rotation is achieved with a flexure hinge at the base of the wing at the interface between the wing and the transmission. A custom-fabrication method (described in Sect. 16.3) enables the designer to create flexures with arbitrary geometries. Incorporated into the wing hinge flexure are joint stops which limit the rotational motion. Therefore, if adequate inertial and aerodynamic loads are experienced by the wing during flapping, the wing

will rotate to a pre-determined angle of attack for each half-stroke.

The statics and dynamics of passive rotation are equally important. Using a pseudo-rigid-body model of the wing hinge flexure, it is simple to estimate the effective torsional stiffness of the wing hinge. Thus for an expected loading we can estimate the maximum rotation angle during flapping. Furthermore, the geometry of the flexure defines the limits of rotation by the joint stops. In order to achieve quasi-static rotation, it is important to also consider the dynamics of the rotational DOF. We design the first rotational resonance to be significantly higher than the flapping resonance by tuning the materials and geometry of the wing and flexure hinge. In this way, the baseline trajectory is mechanically hard coded into the structure and flapping and rotation can be accomplished simultaneously with a single actuator. Derivations from this baseline trajectory – to control body moments – will be accomplished with smaller actuators which subtly alter the transmission of the thorax in a similar manner as Diptera [13].

16.3 Fabrication Using Smart Composite Manufacturing

Because of the scale of the components, we require a 'meso'-scale manufacturing method. 'Meso,' in this use, refers to scales in between two heavily investi regimes: 'macro'-scale (traditional machining) and MEMS. More traditional large-scale machining processes are inappropriate for a robotic insect for two fundamental reasons. First, the required resolution, on the order of 1 μm, would be difficult to achieve with standard machining tools. Second, as the components become smaller, the ratio of surface area to volume increases, and thus surface forces such as friction begin to dominate the dynamics of motion. This latter point implies that more traditional mechanisms for coupling rotations (e.g., sleeve or ball bearings) would exhibit increased inefficiency at the scale of insect joints. Alternatively, researchers have created articulated robotic structures using surface [23] and bulk micromachining [11] MEMS processes. However, MEMS devices are limited in terms of material choice, geometry, and actuation. Furthermore, MEMS process steps typically involve cost-prohibitive infrastructure and significant time delays. For all of these reasons, we require a novel way to construct the articulated and actuated mechanical/electromechanical/aeromechanical components of a robotic insect. This must be fast, inexpensive, repeatable, and result in structures that can have dramatic deformations ($> \pm 60°$), long fatigue life (>10 M cycles), and high power density.

The solution is a multi-step micromachining and lamination process called smart composite microstructures (SCM [21]). In this process, select materials (metals, ceramics, polymers, or fiber-reinforced composites) are first laser micromachined into arbitrary 2D geometries, as shown in Fig. 16.4. This typically involves thin sheets of material and a UV (frequency-tripled Nd:YVO_4, 355 nm) or green (frequency-doubled Nd:YAG, 532 nm) computer-controlled laser. Once each material is cut, they are properly aligned and cured to form the laminate. Alignment can use a number of techniques including folding, fluid surface tension, and mechanical aligners using vision and registration marks (similar to mask aligners). A common constituent lamina material is carbon fiber prepreg. This is a composite material of ultra high modulus fibers with a catalyzed but uncured polymeric matrix. During curing (at elevated temperatures using a modified vacuum bagging process), the matrix flows and makes bonds with the various layers in the laminate. Using this process, we can create laminates with a well-defined spatially distributed compliance (e.g., flexures) which can be folded into any 3D shape with any number of degrees of freedom. Moreover, by including electroactive materials into the laminate – PZT for example – we can create actuators and actuated structures.

This process is the basis for all of the mechanical and aeromechanical components of our robotic flies. It is enabling for the demanding application of a robotic fly and is potentially impactful for a number of other meso-scale robotics applications.

16.4 Actuation and Power

Providing adequate power for lift and thrust is critical for hovering devices. For Dipteran insects, power of 70–100 $W\,kg^{-1}$ of body mass is estimated [16], with power plant power density of approximately 200

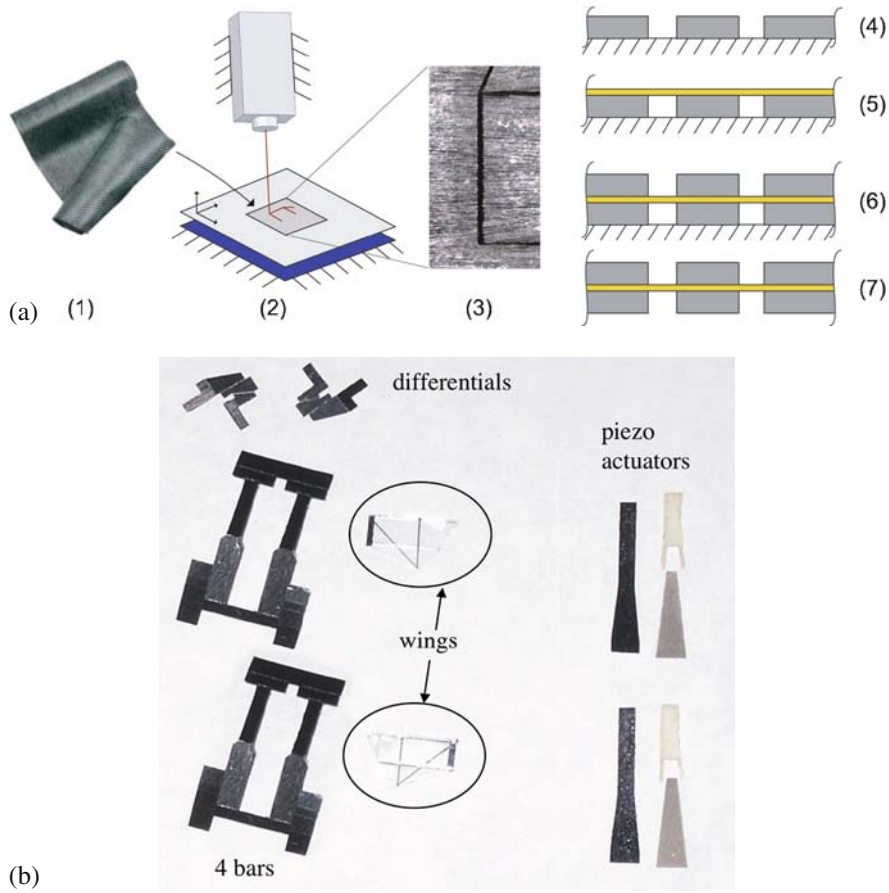

Fig. 16.4 (**a**) Smart composite manufacturing process using laser micromachining and lamination. Gaps are cut in carbon fiber which define flexure joint locations, then an intermediate layer of polyimide is used as the flexure layer, and finally a second layer of carbon fiber is laminated to form the complete structure. (**b**) Example parts for UCB MFI thorax

$\mathrm{W\,kg^{-1}}$. Traditional electromagnetic motors, ubiquitous in larger robotic systems, are inappropriate for actuation of a robotic insect. This is due to the scaling arguments made in Sect. 16.3. Additionally, there are practical limitations to the current density in smaller electromagnetic windings which exacerbate the poor scaling of such motors. (The limits of current available actuators are discussed in Chap. 14 and 21.) Furthermore, a simple periodic (or even harmonic) motion is required to drive the wings. Therefore, any rotary motion would require a kinematic linkage to convert rotations to the flapping motions.

Clamped-free piezoelectric bending bimorph actuators were chosen for the MFI based on the desired metrics of high power density, high bandwidth, high efficiency, and ease of construction [22]. These actuators are constructed using the same method as with the articulated mechanisms; only here some of the constituent layers are piezoelectric. Figure 16.5 shows a cross section of the actuator. Each of the layers is laser micromachined, aligned, and cured in a similar manner as the transmission.

Although initial lift results using piezoelectric actuators were promising [3], verifying actual power output from the actuators is critical for identifying

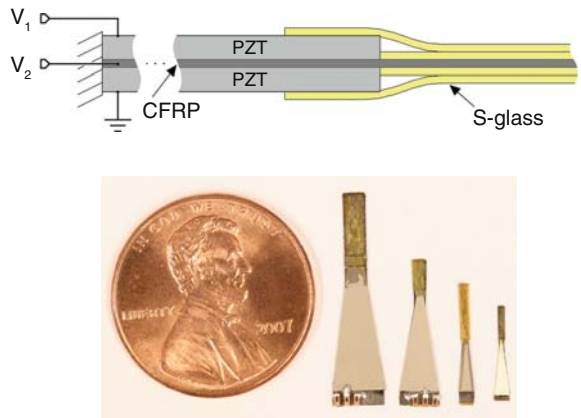

Fig. 16.5 Composite piezoelectric bimorph actuator cross section and example actuators at multiple scales

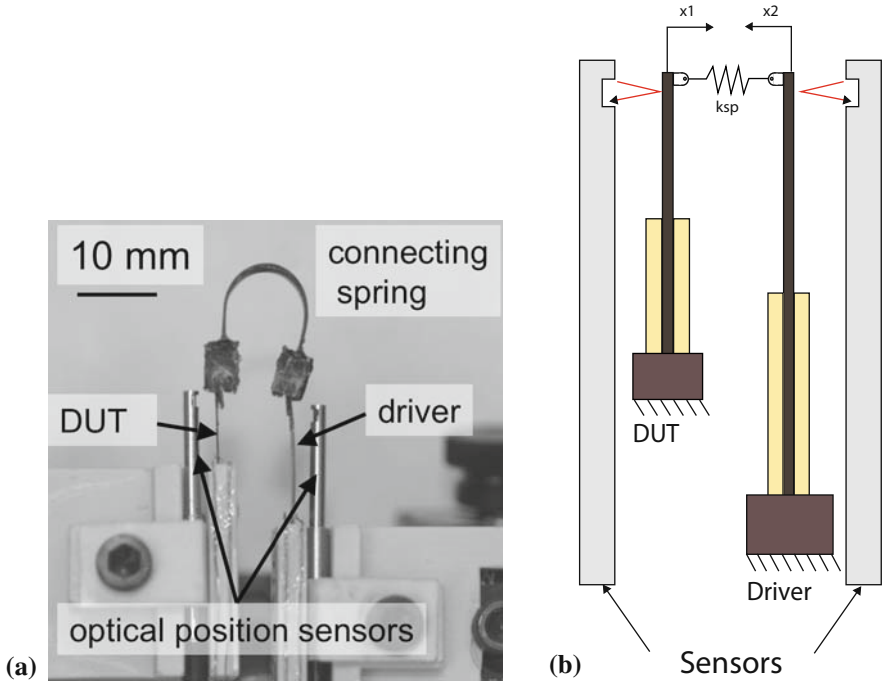

Fig. 16.6 Dynamometer for testing piezoelectric power output at resonance [16]

possible transmission losses or aerodynamic inefficiencies. Extrapolation of actuator performance from DC measurements [22] predicted higher power than was actually observed. Hence, a miniature dynamometer system was developed [16] to measure real actuator output power for simulated damping loads at resonance. Figure 16.6a, b shows the setup for the dynamometer, which uses precision optical sensors to measure the displacement of the drive actuator and the device-under-test (DUT). Force is measured from the extension of the connecting spring, and equivalent damping is set by adjusting the driver phase. As seen in Figure 16.7, with a 10.1 mg actuator, energy density of 1.89 J kg^{-1} was obtained. With operating frequency for the MFI of 275 Hz, power density of 470 W kg^{-1} is obtained, with internal mechanical losses of approximately 10%.

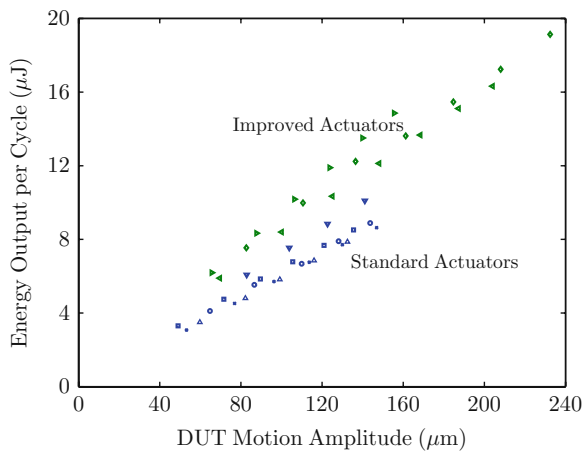

Fig. 16.7 Direct measurements of actuator output energy for various simulated loads at resonance

16.5 Airfoils

Another crucial component of a robotic fly is the airfoils. Insects wings exhibit a huge diversity in shape, size, venation pattern, and compliance. (Wing and aerodynamic issues are considered further in Chaps. 11, 12, and 14.) It is currently unknown how these morphological features affect flight: Are some of the features of insect wings due to bio-material limitations or are they instead an indicator of beneficial performance? Due to the complexity of this question, here current airfoils are designed to match key features of appropriately sized Diptera (aspect ratio, second moment of area, length, etc.) while remaining as rigid and lightweight as possible. To achieve this, carbon fiber 'veins' are laser micromachined and aligned to a

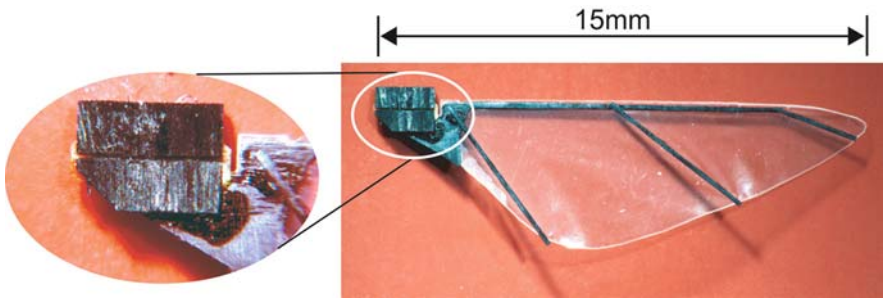

Fig. 16.8 Passive wing hinge with joint stop [19]

thin film polymer membrane (1.5 μm thick polyester) and cured. The outline of the wing shape is then cut with a final micromachining step which results in the wings shown in Fig. 16.8. These airfoils weigh less than 600–700 μg.

16.6 Results

The SCM process and piezoelectric actuators have enabled lightweight thorax designs with both active and passive wing rotation. Active control of wing rotation is possible, but is very sensitive to near exact matching of each half of the thorax structure. Passive wing rotation, while still requiring precise tuning of wing hinge stiffness and rotational inertia properties, is more tolerant of manufacturing process variation.

16.6.1 Dynamic Challenges for Active Control of Flap and Rotation

One of the motivations for active control of wing rotation is the potential to achieve enhanced rotational lift effects at the end of wing strokes [8]. Figure 16.9a shows several candidate wing rotation profiles, including a simple sinusoidal profile and higher harmonics in rotation, to generate a faster wing rotation at the end of each half-stroke. Using a dynamic model of the thorax and wing [14], the required actuator forces can be predicted, as shown in Fig. 16.9b. Interestingly, all the trajectories generate approximately the same lift (within 10%), but the trajectories with the faster rotation require five times greater actuation forces, which exceeds the capabilities of available actuators. This result indicates that a passive rotation, which approximates a sinusoidal rotation, may provide adequate lift forces with minimal power.

16.6.2 MFI Benchtop Lift Test

A benchtop, one-wing version of the MFI was tested using over-sized actuators [14]. Through careful tuning of the amplitude, phase, and frequency of the two actuators (four parameters), an operating point with decent wing rotation was found as shown in Fig. 16.10. Tuning is quite critical, and due to driving at the resonant frequency, controllability is reduced. At 275 Hz, with flap angle ± 35° and rotation ± 45°, a net lift force of 1400 μN was measured using a precision scale. It is interesting to note that the small wing stroke, large wing rotation, high wing-beat frequency used are more bee-like than fly-like [1]. In addition, the high frequency allows better power density from the actuators, and short wing stroke reduces strain on the four bar joints.

16.6.3 Flapping-Wing MAV with Passive Rotation

An alternative design simplifies the thoracic mechanics and uses passive rotation to achieve the required flapping and rotation trajectories. This entails similar components as the active rotation version, but uses only a single actuator and eliminates the differential mechanism. Once the four mechanical and aeromechanical components of the fly (actuator, transmission, airfoils, and airframe) are complete, they are integrated to form the structure in Fig. 16.1b. The first metric of interest is the trajectory that active flapping with

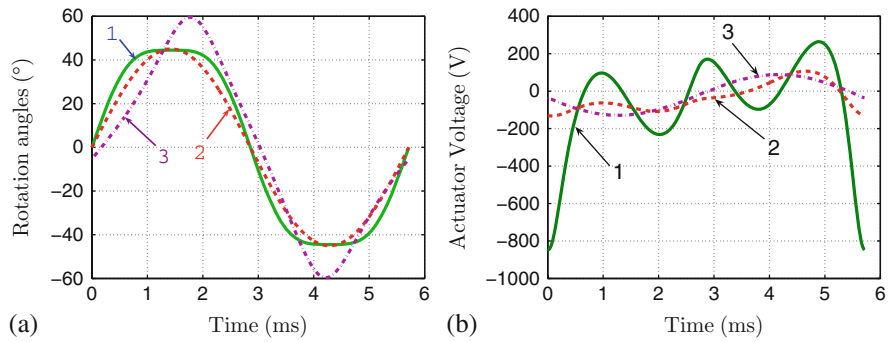

Fig. 16.9 Comparison between desired wing rotations and required actuator voltage. Quick rotations, such as Case 1, require unachievable actuator power, suggesting only slow rotations may be achievable. Case 2 is a pure sinusoid trajectory and Case 3 is a sinusoidal drive voltage. Slow rotations could be achieved by passive aerodynamic and compliant mechanisms [14]

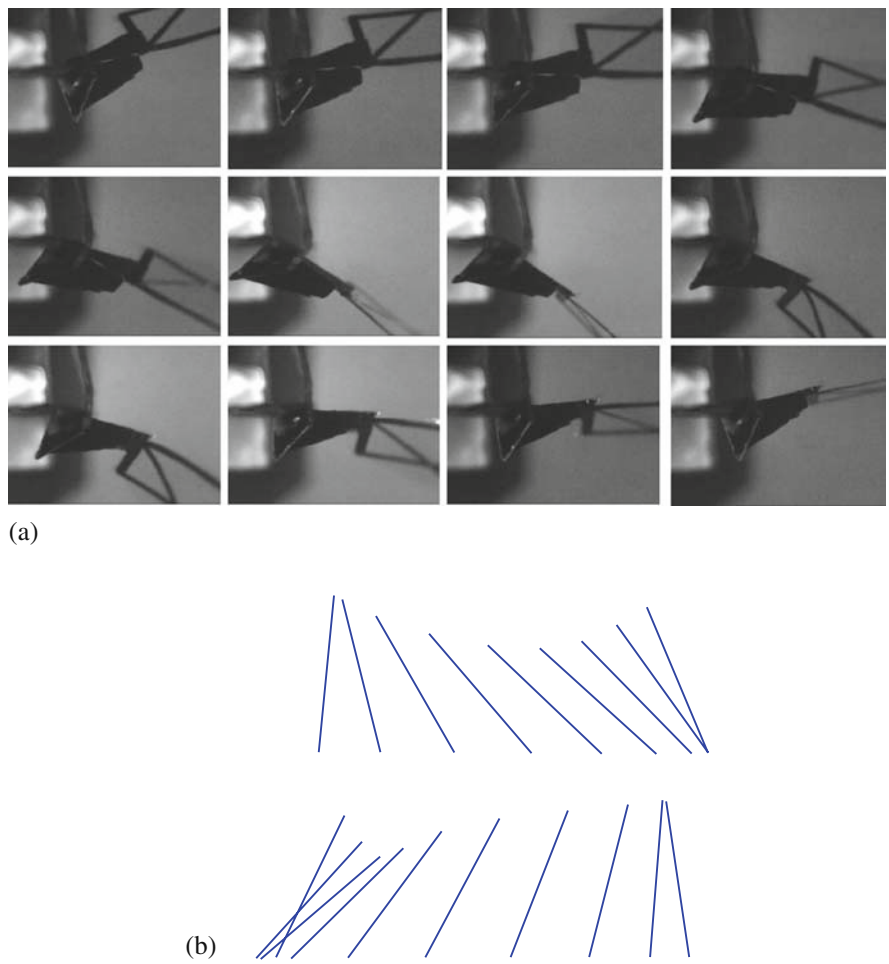

Fig. 16.10 (**a**) Benchtop testing of UC Berkeley MFI [14] with wing beat at 275 Hz. (**b**) Measured wing trajectory in stroke plane

passive rotation can create. This is evaluated by simply driving the wings open loop at the flapping resonant frequency (approximately 110 Hz) and observing the wing motion with a high-speed camera. It was observed that the trajectory is nearly identical to Diptera in hover (see Fig. 16.11a). The second metric of interest is the thrust produced. This was evaluated by fixing the structure to a custom single-axis force transducer and yielded an average thrust-to-weight of approximately 2:1.

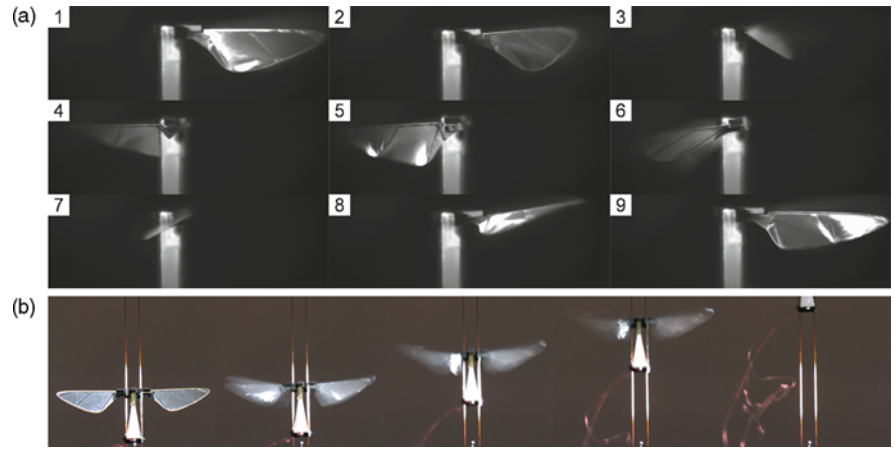

Fig. 16.11 Takeoff of Harvard microrobotic fly

16.6.4 Benchtop Takeoff with Passive Rotation

The final metric for this initial fly is a demonstration of takeoff. The fly was fixed to guide wires which restrict the motion of the fly to purely vertical, the other five body degrees of freedom were constrained. The wings were again driven open loop and the fly ascended the guide wire as shown in Fig. 16.11b. This shows the ability to produce insect-like wing motion with an integrated insect-size robot and that these wing motions produce lift forces of similar magnitude as a similarly sized fly. However, this does not show onboard power, integrated sensors, or automatic control and therefore there are numerous open research questions which need to be addressed to meet the goal of an autonomous robotic insect.

16.7 Conclusion

The two main challenges remaining before free-flying robot flies can be created are flight control and compact power sources. For control, flight stabilization has been shown in simulation [7], and MEMS sensors (body attitude and rate) of the appropriate mass and power are close to off the shelf. While small devices are inherently highly maneuverable due to high angular accelerations (and hence potentially unstable), recent work described in Chaps. 17 points to high damping during turns which may simplify some control issues. Conventional computer vision systems are still too computationally intensive and slow to use on an insect-size flying robot; however, bio-inspired navigation techniques such as optical flow sensing as described in Chaps. 3, 5, and 6 are low mass and can provide crucial flight control information, such as obstacle avoidance.

Power sources currently are the biggest obstacle to 100 mg free flight. The required power source at the 50 mg size is still about an order of magnitude smaller than commercially available practice. The power required for free flight is estimated in Fig. 16.12. For a 100 mg flyer, 10 mW of wing power would provide $100\,\mathrm{W\,kg^{-1}}$ of body mass. Considering thorax losses, and assuming efficient charge recovery [4] from the piezoelectric actuator(s), 27 mW of battery power should be sufficient, which corresponds to a reasonable battery power density of about $600\,\mathrm{W\,kg^{-1}}$ which can be obtained with current LiPoly battery technology (albeit in a 1 g battery rather than the 50 mg battery desired here).

Several key challenges for flapping flight at the 0.1 gram size scale have been met. In particular, thorax kinematics have been designed which can drive wings at high frequency. A new fabrication process, smart composite microstructures (SCM), has enabled lightweight, high-strength, dynamic mechanisms with dozens of joints which can operate at hundreds of Hz, yet weigh only tens of milligrams. These structures have low losses, less than 10%. A low-inertia high stiffness wing has been shown to generate high lift forces. The SCM process has also enabled high-power density piezoelectric actuators, which have demonstrated sufficient power density for lift off of a tethered robot fly.

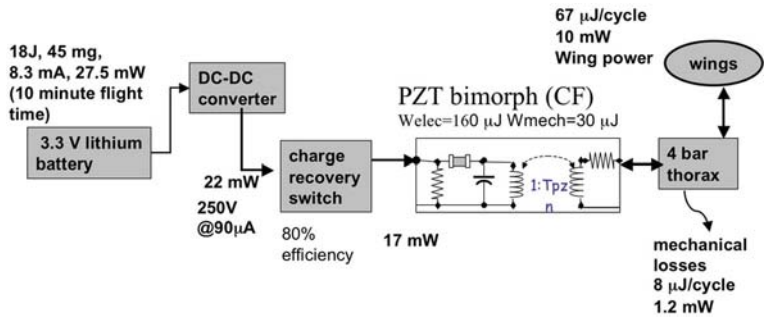

Fig. 16.12 Estimated power budget for free flight of microrobotic fly

We expect that free flight of fly-sized robots should be realizable in the next few years.

Acknowledgments The authors acknowledge the key work of collaborators S. Avadhanula and E. Steltz on thorax and actuator design and characterization. Portions of this work were supported by NSF IIS-0412541. Any opinions, findings, and conclusions or recommendations expressed in this material are those of the author(s) and do not necessarily reflect the views of the National Science Foundation (NSF).

References

1. Altshuluer, D., Dickson, W., Vance, J., Roberts, S., Dickinson, M.: Short-amplitude high-frequency wing strokes determine the aerodynamics of honeybee flight. Proceedings of the National Academy of Sciences (USA) **102**, 18, 213–18, 218 (2005)
2. Avadhanula, S., Wood, R., Campolo, D., Fearing, R.: Dynamically tuned design of the MFI thorax. IEEE International Conference on Robotics and Automation. Washington, DC (2002)
3. Avadhanula, S., Wood, R.J., Steltz, E., Yan, J., Fearing, R.S.: Lift force improvements for the micromechanical flying insect. IEEE/RSJ International Conference on Intelligent Robots and Systems, 2007 IROS 2007 (Oct. 28–30, 2003)
4. Campolo, D., Sitti, M., Fearing, R.: Efficient charge recovery method for driving piezoelectric actuators in low power applications. IEEE Transactions on Ultrasonics, Ferroelectrics and Frequency Control **50**, 237–244 (Mar. 2003)
5. Combes, S., Daniel, T.: Flexural stiffness in insect wings I. Scaling and the influence of wing venation. Journal of Experimental Biology **206** (17), 2979–2987 (2003)
6. Combes, S., Daniel, T.: Flexural stiffness in insect wings II. Spacial distribution and dynamic wing bending. Journal of Experimental Biology **206** (17), 2989–2997 (2003)
7. Deng, X., Schenato, L., Sastry, S.: Model identification and attitude control for a micromechanical flying insect including thorax and sensor models. IEEE Int. Conf. on Robotics and Automation. Taipei, Taiwan (2003)
8. Dickinson, M., Lehmann, F.O., Sane, S.: Wing rotation and the aerodynamic basis of insect flight. Science **284**, 1954–1960 (1999)
9. Dickinson, M., Tu, M.: The function of dipteran flight muscle. Comparative Biochemistry and Physiology vol. 116A, pp. 223–238 (1997)
10. Dudley, R.: The Biomechanics of Insect Flight: Form, Function and Evolution. Princeton University Press (1999)
11. Ebefors, T., Mattsson, J., Kälvesten, E., Stemme, G.: A walking silicon micro-robot. The 10th Int. Conf. on Solid-State Sensors and Actuators (Transducers '99), pp. 1202–1205. Sendai, Japan (1999)
12. Ennos, A.: The inertial cause of wing rotation in Diptera. Journal of Experimental Biology **140**, 161–169 (1988)
13. Miyan, J., Ewing, A.: How Diptera move their wings: A re-examination of the wing base articulation and muscle systems concerned with flight. Philosophical Transactions of the Royal Society of London **B311**, 271–302 (1985)
14. Steltz, E., Avadhanula, S., Fearing, R.: High lift force with 275 hz wing beat in MFI. IEEE/RSJ Int. Conf. on Intelligent Robots and Systems. IROS 2007. pp. 3987–3992 (October 29 2007–November 2 2007)
15. Steltz, E., Avadhanula, S., Wood, R., Fearing, R.: Characterization of the micromechanical flying insect by optical position sensing. IEEE International Conference on Robotics and Automation. Barcelona, Spain (2005)
16. Steltz, E., Fearing, R.: Dynamometer power output measurements of piezoelectric actuators. IEEE/RSJ Int. Conf. on Intelligent Robots and Systems. IROS 2007. pp. 3980–3986 (October 29 2007–November 2 2007)
17. Sunada, S., Ellington, C.: A new method for explaining the generation of aerodynamic forces in flapping flight. Mathematical Methods in the Applied Sciences **24**, 1377–1386 (2001)
18. Wang, Z., Birch, J., Dickinson, M.: Unsteady forces and flows in low reynolds number hovering flight: two-dimensional computations *vs* robotic wing experiments. Journal of Experimental Biology **207**, 449–460 (2004)
19. Wood, R.: Design, fabrication, and analysis of a 3dof, 3 cm flapping-wing MAV. IEEE/RSJ Int. Conf. on Intelligent Robots and Systems, 2007. IROS 2007. pp. 1576–1581 (October 29 2007-November 2 2007)

20. Wood, R., Avadhanula, S., Menon, M., Fearing, R.: Microrobotics using composite materials: The micromechanical flying insect thorax. IEEE Int. Conf. on Robotics and Automation. Taipei, Taiwan (2003)
21. Wood, R., Avadhanula, S., Sahai, R., Steltz, E., Fearing, R.: Microrobot design using fiber reinforced composites. Journal of Mech. Design **130** (5) (2008)
22. Wood, R., Steltz, E., Fearing, R.: Optimal energy density piezoelectric bending actuators. Journal of Sensors and Actuators A: Physical **119** (2), 476–488 (2005)
23. Yeh, R., Kruglick, E., Pister, K.: Surface-micromachined components for articulated microrobots. Journal of Microelectrical Mechanical Systems **5** (1), 10–17 (1996)